PSFC/JA-10-48

Spherical conducting probes in finite Debye length plasmas and ExB fields

L. Patacchini & I. H. Hutchinson

December 2010

Plasma Science and Fusion Center
Massachusetts Institute of Technology
Cambridge MA 02139 USA

Submitted for publication to *Plasma Physics and Controlled Fusion*.

This work was supported in part by the U.S. Department of Energy, Grant No. DE-FG02-06ER54891.

Spherical conducting probes in finite Debye length plasmas and $\mathbf{E} \times \mathbf{B}$ fields

Leonardo Patacchini and Ian H. Hutchinson

Plasma Science and Fusion Center, MIT

Abstract

The particle in cell code SCEPTIC3D [Patacchini and Hutchinson, *Plasma Phys. Control. Fusion* **52** 035005 (2010)] is used to calculate the interaction of a transversely flowing magnetized plasma with a negatively charged spherical conductor, in the entire range of magnetization and Debye length. The results allow the first fully self-consistent analysis of probe operation where neither the ion Larmor radius nor the Debye length are approximated by zero or infinity. An important transition in plasma structure occurs when the Debye length exceeds the average ion Larmor radius, as the sphere starts to shield the convective electric field driving the flow. A remarkable result is that in those conditions, the ion current can significantly exceed the unmagnetized orbital motion limit. When both the Debye length and the Larmor radius are small compared to the probe dimensions however, their ratio does not affect the collection pattern significantly, and Mach probe calibration methods derived in the context of quasineutral strongly magnetized plasmas [Patacchini and Hutchinson *Physical Review E* **80**, 036403 (2009)] hold for Debye lengths and ion Larmor radii smaller than about 10% of the probe radius.

1 Introduction

In a recent publication [1], the three-dimensional extension to the specialized coordinate electrostatic particle and thermals in cell (SCEPTIC) code [2, 3, 4, 5], SCEPTIC3D, was used to study the interaction of an ion-collecting sphere with a transversely flowing collisionless magnetoplasma, in the zero-Debye length (quasi-neutral) approximation. We here report new insights obtained in the entire range of Debye length to sphere radius ratio.

Collisionless ion collection by spherical objects is a long-studied classic of plasma physics [6], the treatment of which requires self-consistent solution of the ion dynamics and the electrostatic potential distribution (The electrons are usually taken as Boltzmann distributed around ion-attracting objects [7].). This is a complex non-linear problem that only recent computational power allows to fully tackle. Figure (1) shows the physical parameter-space projected on the Λ_{De}/R_p–R_L/R_p plane, where Λ_{De}/R_p and R_L/R_p are the ratios of electron Debye length and average ion Larmor radius to the probe radius, respectively. Analytic, semi-analytic and earlier computational treatments (usually) need to simplify the physics by letting one or two of those dimensionless parameters go to zero or infinity.

When $R_L/R_p \gg 1$, the ions can be treated as unmagnetized because their Larmor radius is much larger than the extent of the probe-induced potential perturbation. In the further limit $\Lambda_{De}/R_p \gg 1$ the probe is unshielded and the potential perturbation adopts a vacuum (Coulomb) form. The analytic Orbit Motion Limited (OML) solution (based on angular momentum conservation), derived

by Mott-Smith and Langmuir in the 1920s [8] in the case of stationary plasmas, and later by Kanal [9] in the presence of flow, here applies. This is region 1 in Fig. (1). Reversing the latter of the two limits to where $\Lambda_{De}/R_p \ll 1$ (region 2), the probe is strongly shielded and the quasineutral plasma region extends down to an infinitesimally thin Debye layer at its surface. For stationary plasmas in the cold-ion limit, the problem was first formalized and solved analytically by Bohm for mono-energetic ions in 1949. For a more recent review see for example Ref. [10]. The remaining unmagnetized regimes are not analytically tractable. Situations where Λ_{De} cannot be neglected (region 3) are physically complex, because Poisson's equation for the electrostatic potential must be solved in the entire perturbed region. An important contribution was the numerical solution of the stationary problem by Laframboise in the 1960s [11], but not until recently was the drifting regime definitively explored through Particle In Cell (PIC) simulations [2, 3].

Treatments accounting for finite ion magnetization are rare and quite recent, as they require the computationally expensive integration of magnetized orbits; the vacuum limit problem (region 4) without drift was solved in 1991 by Sonmor and Laframboise [12]. When $R_L/R_p \ll 1$, the ions are strongly magnetized and their motion outside a thin magnetic presheath layer can be treated in the drift approximation. In the further limit $\Lambda_{De}/R_p \ll 1$ (region 5) the plasma region of interest is quasineutral; solutions can then be found semi-analytically by the method of characteristics [13], or analytically upon approximating the ions as isothermal [14]. The strongly magnetized non-zero Debye length case (regions 7 and 8) can also be treated in the drift approximation, although to our knowledge no publication taking advantage of this property is available.

One of the original motivations for developing SCEPTIC3D was to study Mach probes in tokamak edge plasmas, where the electron Debye length Λ_{De} is usually one order of magnitude smaller than R_L, itself about one order of magnitude smaller than R_p (Table 1 shows "typical" mid-plane scrape off layer values of R_L and Λ_{De} for Alcator C-Mod and DIII-D.). Mach probes seek to measure the unperturbed (or external) plasma velocity by comparing ion flux-densities Γ_i in different directions, with the relationship between measurements and flow being referred to as the "calibration" [7]. In the unmagnetized regime (region 2) the spherical probe problem has azimuthal symmetry around the velocity axis, and measuring the upstream to downstream flux ratio $R = \Gamma_i^{\mathrm{Up}}/\Gamma_i^{\mathrm{Do}}$ is sufficient to calculate the unperturbed flow Mach number M [2]. In the opposite limit of strong magnetization (region 5), each plane parallel to flow and magnetic field can be treated independently [13, 14]; parallel and transverse Mach numbers M_∞ and $M_\perp$ with respect to the magnetic field can therefore be obtained by flux measures at different angles in a *single* such plane. Within the same zero-Debye length approximation yet when the ion Larmor radius compares to the probe radius (region 6), the plasma profiles show a complex three-dimensional structure. A major result of Ref. [1] obtained with SCEPTIC3D was that regardless of the magnetic field strength, a transverse Mach probe with four electrodes placed at 45^o to the magnetic field in a plane of flow and magnetic field could be calibrated with a single probe-shape-dependent factor M_c: a function of ion temperature and magnetic field only (Eqs (20,21)).

When the zero-Debye length approximation does not hold, the probe negative bias permeates in the plasma region over a distance $\sim \Lambda_{De}$. Hence, for large enough Λ_{De} ions tend to have more complex orbits, and information on the unperturbed drift gets "lost". This is true in unmagnetized plasmas [3] (region 3), but even more so in the magnetized regime as the conducting probe shields the convective electric field driving the transverse drift (region X in Fig. (1)). The purpose of this publication is to investigate this finite magnetization and Debye length regime with SCEPTIC3D, i.e. the shaded region of the parameter-space shown in Fig. (1), and its connection to all known

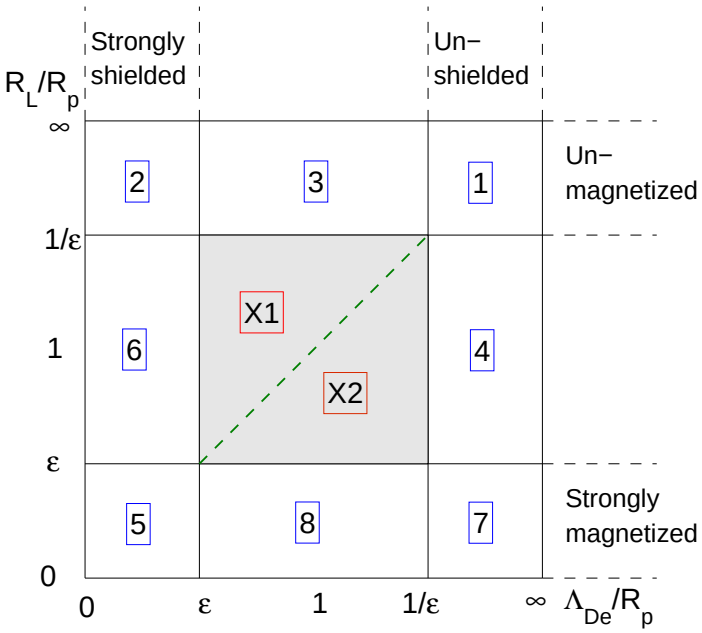

Figure 1: Parameter-space projected on the dimensionless length-scale plane Λ_{De}/R_p–R_L/R_p. ε is formally intended as tending to zero. The central shaded region, where neither Λ_{De} nor R_L can be approximated by zero or infinity with respect to the probe radius R_p, is where the focus of this publication lies. See the main text for a description of the numbered regions.

	T_e (eV)	T_i (eV)	B (T)	n_e (m^{-3})	R_L (μm)	Λ_{De} (μm)	Object	Regions (Fig. (1))
MP SOL Alcator C-Mod	20	20	5	$2 \cdot 10^{19}$	115	7.4	Dust Probe	1, 3, X1 5, 6, X1
MP SOL DIII-D	10	10	2	$5 \cdot 10^{18}$	203	10.5	Dust Probe	1, 3, X1 5, 6, X1
Ion-drag exp.	1.7	0.03	0	$1.49 \cdot 10^{16}$	∞	79.4	Dust Probe	1, 3 2

Table 1: Negatively charged spheres can model dust particles (radius $R_p \sim 1 - 200\mu$m) as well as flux-sensing probes ($R_p \sim$ 1-5mm) in a variety of plasma conditions. The first two lines show "typical" Mid-Plane Scrape Off Layer (MP SOL) parameters for Hydrogen discharges in the Alcator C-Mod and DIII-D tokamaks [15]; the third is taken from an unmagnetized ion-drag force measurement experiment by Nosenko and coauthors [16].

limiting solutions in Λ_{De}/R_p and R_L/R_p.

Our calculations are also of interest to the study of dust, occurring quite often in astrophysical contexts as well as in industrial and laboratory plasmas. In particular, dust is commonly found in magnetic confinement fusion devices, where disruptions, ELMs and other violent events can erode micrometer or even millimeter-size chips [17]. Most situations involve dust whose radius compares to or is smaller than the average ion Larmor radius, and where $R_L \gtrsim \Lambda_{De}$ (see Table 1), i.e region X_1 in Fig. (1). We are not aware of experiments involving probes or dust in a plasma with $R_L \lesssim \Lambda_{De}$, hence region X2 is perhaps of lesser practical interest today. It is very likely however that following the strong recent interest in cold dusty plasmas [18], magnetized experiments in this regime will be performed in the near future.

A review of the SCEPTIC3D code as well as a discussion of the aspects specific to the finite Debye length operation are given in section 2. We then proceed with the results concerning the plasma profiles (section 3), the ion current (section 4) and Mach probe calibration (section 5).

2 Model and computational method

2.1 Problem formulation

We focus on a negatively charged spherical conductor of radius R_p, referred to as "probe", "electrode", "dust" or "sphere", placed in a Maxwellian plasma of monoionized ions (charge Z and mass m) and electrons. A uniform background magnetic field $\mathbf{B}$ and a uniform convective electric field $\mathbf{E}_{\text{conv}}$ drive an external "$\mathbf{E} \times \mathbf{B}$" drift $\mathbf{v}_\perp = \mathbf{E}_{\text{conv}} \times \mathbf{B}/\mathbf{B}^2$. Adding a free parallel drift $\mathbf{v}_\infty = v_\infty \mathbf{B}/B$, the total velocity of the *unperturbed* plasma is $\mathbf{v_d} = \mathbf{v}_\perp + \mathbf{v}_\infty$.

We define the unperturbed ion and electron charge-densities $ZN_i = N_e = N_\infty$, and unperturbed temperatures $T_{i\infty}$ and T_e. R_p can take any value with respect to the *unperturbed* electron Debye length $\Lambda_{De} = \left(\epsilon_0 T_e / e^2 N_\infty\right)^{1/2}$ and the average ion Larmor radius at infinity $R_L = \left(\pi m T_{i\infty}/2\right)^{1/2} / \left(ZeB\right)$, but is much smaller than $\Lambda_{De} c/c_{s0}$ (c is here the speed of light, and c_{s0} the cold-ion sound speed defined in Eq. (3)) so that the magnetic field distribution in the plasma is unperturbed. The probe however induces a potential perturbation Φ, satisfying Poisson's

equation, such that the total electric field at any given point in space is

$$\mathbf{E} = \mathbf{E}_{\text{conv}} - \nabla\Phi; \tag{1}$$

it is this *total* electric field that acts on each ion, whose position $\mathbf{x} = (x, y, z)^T$ obeys Newton's equation

$$\frac{m}{Ze}\frac{\mathrm{d}^2\mathbf{x}}{\mathrm{d}t^2} = \mathbf{E} + \frac{\mathrm{d}\mathbf{x}}{\mathrm{d}t} \times \mathbf{B}. \tag{2}$$

The unperturbed plasma being uniform, external diamagnetic drifts in the presence of transverse pressure gradients are not modelled; the code will only capture local diamagnetic drifts arising from the probe-induced density and temperature perturbations. Also not modelled are "$\nabla\mathbf{B}$" drifts, certainly important for the plasma dynamics in tokamaks, but whose effects on Mach probe measurements have not received much theoretical attention sofar. Inclusion of those additional external drifts in the SCEPTIC3D code will be considered for future work.

The probe surface behaves as an ideal ion and electron sink. Global charge conservation in the system "plasma+probe" therefore imposes internal current densities of the order $eN_\infty c_{s0}$, where

$$c_{s0} = \left(\frac{ZT_e}{m}\right)^{1/2} \tag{3}$$

is the cold-ion sound speed. Neglecting the Hall term and taking its conductivity large enough, the probe can be treated as an equipotential, i.e. $\mathbf{E}_{\text{conv}} - \nabla\Phi(R_p, s) = 0$ where "s" is a surface parameterization.

Because most (fully) analytic results concerning Mach probes have been derived with the approximation of isothermal ions [14, 19], we use as Mach numbers "M" velocity divided by the isothermal ion sound speed

$$c_{sI} = \left(\frac{ZT_e + T_{i\infty}}{m}\right)^{1/2}. \tag{4}$$

The median probe bias Φ_p, hereafter referred to as "the probe bias" for simplicity, is assumed to be negative enough for $|\mathbf{E}_{\text{conv}}R_p| + \Phi_p$ to be negative by a few T_es (typically $|\mathbf{E}_{\text{conv}}R_p| + \Phi_p \lesssim -2T_e/e$), so that the entire probe surface is strongly electron-repelling. Approximating the electrons as massless, their momentum equation can easily be integrated along the magnetic field lines upon neglecting the acceleration term. This yields isothermal electrons (hence the lighter notation T_e for $T_{e\infty}$) with Boltzmann density

$$N_e = N_\infty \exp\left(\frac{e\Phi}{T_e}\right), \tag{5}$$

down to a thin layer at the probe surface [1], where a significant fraction of the electron orbits (the outgoing orbits) is empty. The electron density is however negligible there, thus considering Eq. (5) to be valid in the entire domain does not affect electrostatic potential or ion current computations.

Non-thermal electron effects, such as the presence of a hot energetic tail in their distribution function, would require a modification of Eq. (5) (see for instance Ref. [20]) and are not modelled in this publication.

2.2 Code operation

Comprehensive description and benchmarking of SCEPTIC3D in the zero-Debye length limit is available to the reader in Ref. [1], and for brevity we here discuss only the aspects specific to finite Debye length operation.

SCEPTIC3D is a 3D3v hybrid electrostatic Particle In Cell (PIC) code [21, 22] with Lagrangian ions governed by Eq. (2), and isothermal electrons with Boltzmann density given by Eq. (5). Its spatial domain is represented in spherical coordinates, as illustrated in Fig. (2). The radial distance measured from the probe center, R, is conformal to the probe surface; $\theta \in [0:\pi]$ is the polar angle measured from the magnetic axis ($\mathbf{e_z}$); and $\psi \in [0:2\pi]$ is the azimuthal angle measured from the plane of convective and magnetic fields (the $\{\mathbf{e_x}, \mathbf{e_z}\}$-plane). The grid is uniformly spaced in R, $\cos\theta$ and ψ. The angle between $\mathbf{B}$ and $\mathbf{v_d}$ is denoted δ.

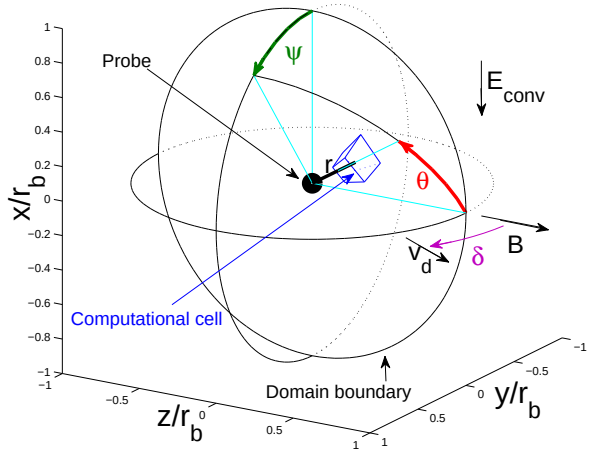

Figure 2: Three-dimensional view of SCEPTIC3D's computational domain (from Ref. [1]).

The code uses non-dimensional quantities. The potential ϕ is in units of T_e/e, distances in probe radii, and charge-densities in N_∞. Dimensionless distances and densities are indicated by lower-case characters ($\lambda_{De} = \Lambda_{De}/R_p$, $n_i = ZN_i/N_\infty$, etc.). Results in the large Debye length limit will often be interpreted in terms of $\chi = -\phi/\tau$, where $\tau = T_{i\infty}/ZT_e$ is the thermal energy ratio at infinity:

$$\phi = \frac{e\Phi}{T_e}, \qquad \chi = -\frac{Ze\Phi}{T_{i\infty}}. \tag{6}$$

We also define velocities "w" normalized to the ion thermal speed $v_{ti} = (2T_{i\infty}/m)^{1/2}$: $w_{\infty,\perp,d} = v_{\infty,\perp,d}/v_{ti}$, and the magnetic field strength as the ratio of the probe radius to the mean ion Larmor radius at infinity

$$\beta_i = \frac{R_p}{R_L} = ZeBR_p\left(\frac{2}{\pi m T_{i\infty}}\right)^{1/2}. \tag{7}$$

Charge flux-densities will be scaled to the random thermal charge flux-density $\Gamma_i^0 = N_\infty v_{ti}/(2\sqrt{\pi})$, and currents to $I_i^0 = 4\pi R_p^2 \Gamma_i^0$.

Upon normalizing "∇" by $1/R_p$, Poisson's equation for the electrostatic potential becomes:

$$\nabla^2\phi = \frac{\exp\phi - n_i}{\lambda_{De}^2}. \tag{8}$$

Rather than solve the nonlinear equation, Eq. (8), at each PIC timestep, we assume that the potential changes only slightly each step. If ϕ^* is the known potential distribution at time-step t and ϕ the unknown distribution at time-step $t+1$, we can linearize Eq. (8) about ϕ^*:

$$\nabla^2\phi = \frac{\exp(\phi^*)\left[1+(\phi-\phi^*)\right] - n_i}{\lambda_{De}^2}. \tag{9}$$

We then discretize Eq. (9) to the second order by finite volumes, according to which we look for a potential distribution ϕ such that for each computational cell,

$$\int_{\text{Cell boundary}} \nabla\phi\cdot\mathrm{d}\mathbf{S} = \frac{1}{\lambda_{De}^2}\int_{\text{Cell}} \left\{\exp(\phi^*)\left[1+(\phi-\phi^*)\right] - n_i\right\}\mathrm{d}\Omega. \tag{10}$$

The discretized operator on ϕ corresponding to Eq. (10) is sparse (with 7-point stencil) and symmetric, but not definite positive. For its inversion, we developed a *fully parallelized* block-solver based on the *minimum residual* method. The algorithm implementation, completed by a straightforward Jacobi preconditioning, is mostly adapted from chapter 2.7 in Ref. [23]. The domain is split for the Poisson solver in a way that minimizes the number of interfaces.

A "typical" production run is performed with approximately 50M computational ions, distributed on 128 cores of the MIT PSFC Parallel Opteron/Infiniband cluster Loki. The choice of grid depends on the specifics of the run, in particular the Debye length, as it is important not to over-resolve the domain. Indeed even a modest grid of $100\times30\times30$ ($r\times\theta\times\psi$) has 90k cells. The total cost (particle mover + Poisson solver) is less than half a second per time-step, which allows most datasets to run in less than one hour (usually between 2k and 8k time-steps are required, depending on the ion temperature and the domain-size).

2.3 Boundary conditions

Solution of Eq. (8) requires two boundary conditions. The inner condition straightforwardly arises from the conducting probe potential distribution, which can be decomposed into a monopole term Φ_p and a dipole-like term $|\mathbf{E}_{\text{conv}}R_p|$ oriented in the $\mathbf{e_x}$ direction ($\mathbf{E}_{\text{conv}} = E_{\text{conv}}\mathbf{e_x}$ with $E_{\text{conv}}<0$). In dimensionless form and spherical coordinates:

$$\phi(R_p,\theta,\psi) = \phi_p + \frac{e}{T_e}\left[E_{\text{conv}}R_p\right]\sin\theta\cos\psi. \tag{11}$$

The sphere median potential, ϕ_p, is specified as an input. The outer condition on ϕ uses an approximation designed to model most economically for unmagnetized plasmas the connection to the unperturbed plasma (See Ref. [3] for details.). It works with magnetized plasmas provided the entire sheath is included in the computational domain (qualitatively $r_b \gtrsim \max 4\,(r_p,\lambda_{De})$), because it ensures quasineutrality ($n_i = n_e = \exp(\phi)$) at the outer boundary regardless of the magnetic field.

The reinjection scheme and particle count is the same as Ref. [1]. When an ion is collected by the probe or freely leaves the computational domain, it is randomly reinjected at the outer boundary

from an *unperturbed* Maxwellian distribution with temperature $T_{i\infty}$ and drift velocity $\mathbf{v_d}$. Of course the downstream region is perturbed by the probe, and the ion distribution function there is far from Maxwellian. However, because information cannot propagate against the cross-field drift on a scale longer than R_L or Λ_{De}, the saturation current will nevertheless be correct provided each ion collected by the probe entered the computational domain from an unperturbed plasma region. This condition is met for large enough computational domains, qualitatively $r_b \gtrsim 2/M_\perp$ [1].

In summary, the requirement on the computational domain size is $r_b \gtrsim \max(4r_p, 4\lambda_{De}, 2/M_\perp)$.

3 Plasma profiles

3.1 Beads on a wire

SCEPTIC3D can treat arbitrary electron Debye lengths and ion Larmor radii, a capability that will extensively be used throughout this publication. Preliminary insight on shielding effects can however be obtained by a much simpler drift (or "beads on a wire") analysis, appropriate when the ion Larmor radius is much smaller than the probe radius. Perpendicular motion can then be approximated as the drift $(v_x, v_y)^T = \mathbf{E}\times\mathbf{B}/B^2$. The parallel (to $\mathbf{B}$) ion distribution function f is therefore the solution of the 1D kinetic equation

$$v_z\frac{\partial f}{\partial z} + v_x\frac{\partial f}{\partial x} + v_y\frac{\partial f}{\partial y} - \frac{Ze}{m}\frac{\partial \Phi}{\partial z}\frac{\partial f}{\partial v_z} = 0, \tag{12}$$

showing that f is conserved along $(x, y, z, v_z)^T$ orbits that satisfy

$$\frac{\mathrm{d}}{\mathrm{d}t}\begin{Bmatrix} x \\ y \\ z \\ v_z \end{Bmatrix} = \begin{Bmatrix} v_x \\ v_y \\ v_z \\ -\dfrac{Ze}{m}\dfrac{\partial\Phi}{\partial z}. \end{Bmatrix} \tag{13}$$

The ion-charge density distribution, required in Poisson's equation to compute the electrostatic potential Φ self-consistently governing the orbits (13), can be obtained by tracing back those same orbits to infinity where the ion distribution function is (a shifted) Maxwellian. For simplicity we here only discuss the two limiting regimes in Λ_{De} where Poisson's equation need not be solved.

3.1.1 Review of the quasineutral limit

When $(\Lambda_{De}, R_L) \ll R_p$ (region 5), the strongly magnetized ions are governed by Eq. (12) with uniform $v_x = 0$ and $v_y = v_\perp$, and a self-consistent quasineutrality potential $\Phi = T_e/e \ln\left(\int f(v_z)\,\mathrm{d}v_z\right)$, down to a thin layer at the probe surface of width $\sim \max(\Lambda_{De}, R_L)$. If $\Lambda_{De} \lesssim R_L$, the first approximation to break down as we approach the probe is the uniform transverse drift; if $R_L \lesssim \Lambda_{De}$, it is quasineutrality. In either case the Debye and magnetic sheaths need not be resolved because they are infinitesimally thin. If the parallel ion distribution f at the *sheath entrance* is known, it can be integrated to obtain the parallel fluid velocity there, and combined with the unperturbed cross-field velocity. This is Eq. (17) in Ref. [13], yielding the ion collection per unit time, per unit area perpendicular to $\mathbf{B}$, $\Gamma_{i\parallel}$.

Because $v_x = 0$ (in the region of interest), and quasineutrality is a local condition, planes of field and drift are independent. This problem has been solved analytically in the isothermal ion approximation [14], and semi-analytically by the method of characteristics accounting for self-consistent temperature profiles [13].

3.1.2 Vacuum limit

When $R_L \ll (R_p, \Lambda_{De})$ (regions 7 and 8), the Debye sheath has to be resolved, and spatial variation in drift velocity $(v_x, v_y)^T$ must be taken into account.

For purposes of comparison with SCEPTIC3D, we observe that, in the vacuum limit, i.e. $R_p \ll \Lambda_{De}$ (region 7), Poisson's equation need not be solved and the probe-induced potential distribution is simply the sum of a monopole and dipole:

$$\Phi = \Phi_p \frac{R_p}{R} + [E_{\rm conv} R_p] \frac{R_p^3}{R^3}\, x. \tag{14}$$

The *total* drift required to integrate the orbits (13) is then given by $v_y = v_\perp + (\partial\Phi/\partial x)/BR_p$ and $v_x = -(\partial\Phi/\partial y)/BR_p$:

$$v_y = v_\perp \left(1 - \frac{R_p^3}{R^3} + \frac{\Phi_p}{[E_{\rm conv} R_p]} \frac{R_p^3}{R^3}\, x + 3\frac{R_p^5}{R^5}\, x^2 \right), \tag{15}$$

$$v_x = -v_\perp \left(\frac{\Phi_p}{[E_{\rm conv} R_p]} \frac{R_p^3}{R^3}\, y + 3\frac{R_p^5}{R^5}\, xy \right). \tag{16}$$

An important point to notice from Eqs (15,16) is that the drift vector $(v_x, v_y)^T$ at $R = R_p$ is tangent to the probe surface, because the total electric field is normal. Strongly magnetized ions in *non-zero Debye length* plasmas are collected with pure parallel velocity. As a result, if the parallel ion-charge distribution f at the *probe surface* is known, the ion collection per unit time, per unit area perpendicular to $\mathbf{B}$ is given by

$$\Gamma_{i\parallel} = \begin{cases} -\displaystyle\int_{v_z<0} v f(v_z) \mathrm{d}v_z & \text{if } \ z \geq 0, \\ \displaystyle\int_{v_z>0} v f(v_z) \mathrm{d}v_z & \text{if } \ z \leq 0. \end{cases} \tag{17}$$

Note that unlike the quasineutral formula (17) in Ref. [13], the external cross-field velocity $v_\perp$ does not enter Eq. (17) of the present work.

The local parallel ion distribution function in Eq. (17) is obtained by tracing back to infinity each orbit having an inward velocity. We use the Matlab built-in function "ode45", which is an adaptive fourth or fifth order Runge Kutta scheme.

In this vacuum limit the electron dynamics is irrelevant, so collected ion flux-densities normalized to $\Gamma_i^0 = N_\infty v_{ti}/(2\sqrt{\pi})$ will only depend on the dimensionless ion parameters $w_\perp$, w_∞, χ_p and β_i. Figure (3) shows a selection of ion (guiding-center) orbits integrated backwards from two different positions on the sphere surface, using the parameters $\chi_p = 10$, $\beta_i = 50$, $w_\perp = 0.5$ and selected values of w_0. The parallel external drift w_∞ does not enter the orbit equation, but governs the phase-space density associated with each orbit, hence the collected ion current. Rewriting the convective

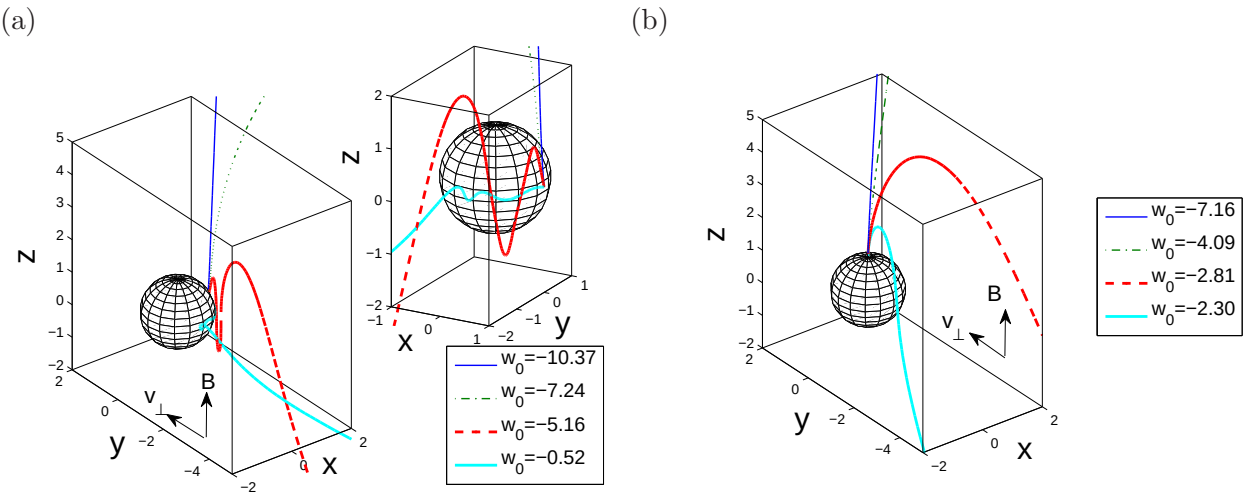

Figure 3: Selection of 3D ion guiding-center orbits, solutions of Eqs (13), traced backwards from the probe surface at (a) $x = 1$, $z = 0^+$ and (b) $x = 0$, $y = 0$, $z = 1$. $w_0 = v_0/v_{ti}$ is the "final" backwards parallel velocity of the considered orbit. The simulation parameters for those plots are $\chi_p = 10$, $\beta_i = 50$, and $w_\perp = 0.5$. Notice that in this figure, the z (magnetic)-axis is oriented vertically. In (a), two different views of the same orbits are proposed.

electric field in ion thermal units ($E_{\rm conv}/\left(T_{i\infty}/Ze\right) = -\sqrt{\pi} w_\perp \beta_i / R_p$) shows that part of the sphere becomes ion-repelling when $\sqrt{\pi}|w_\perp|\beta_i \geq \chi_p$, which is the case with our choice of parameters: $\chi(R_p) \in [\chi_p - \sqrt{\pi}|w_\perp|\beta_i : \chi_p + \sqrt{\pi}|w_\perp|\beta_i] \simeq [-3.43 : 5.43] \cdot \chi_p$. Although not a realistic situation (probes usually operate in the fully electron-repelling regime, and a dust particle's floating potential will adjust to a value negative enough such that electrons are repelled on its entire surface), it helps introduce important concepts by "exaggerating" physical effects.

Orbits whose "end" is on the ion-attractive side (Fig. (3a)) can either trace back to infinity if their velocity (parallel to $\mathbf{B}$) at the probe $w_0 = v_0/v_{ti}$ is inwards enough, or reintersect the probe otherwise, in which case they do not contribute to the ion current. For this particular example ("end" at $x = 1$, $z = 0^+$), the orbit with $w_0 = -0.52$ is a limiting case since it closely (backwards) follows the probe surface until it reaches the ion-repelling side, and then picks up the cross-field velocity $w_\perp$. Orbits with smaller $|w_0|$ close on the sphere, and are thus unpopulated.

Orbits in Fig. (3b), ending at ($x = 0$, $y = 0$, $z = 1$), are simpler. In either case however, it is clear that the ion guiding centers are not confined on a plane of magnetic field and external drift as in the quasineutral regime later illustrated in Fig. (13).

The drift model is valid in the "zero" (with respect to the probe dimensions) Larmor radius limit, but we need to account for finite β_i in order to keep $\mathbf{E}_{\rm conv}$ finite. This was not necessary in the quasineutral limit because the probe shielding of $\mathbf{E}_{\rm conv}$ was confined in the infinitesimal sheath.

Equation (17) will be used in the discussion of current collection and Mach-probe calibration (sections 4 and 5). We now show plasma profiles in the strongly magnetized regime computed using SCEPTIC3D, bridging between the just discussed quasineutral and vacuum limits.

(a) $\lambda_{De} = 0.03$

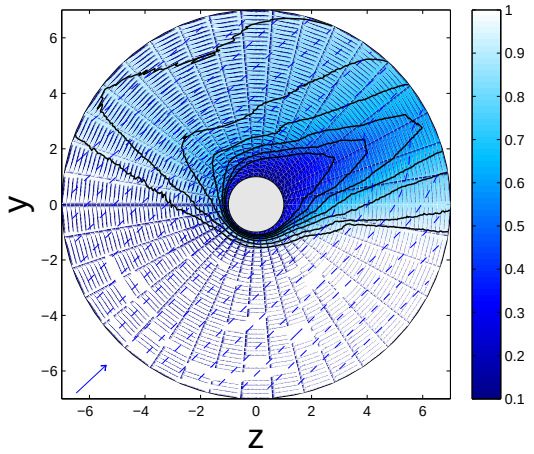

(b) $\lambda_{De} = 0.1$

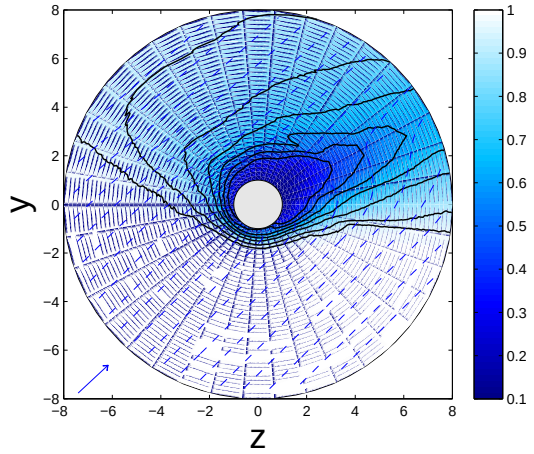

(c) $\lambda_{De} = 0.3$

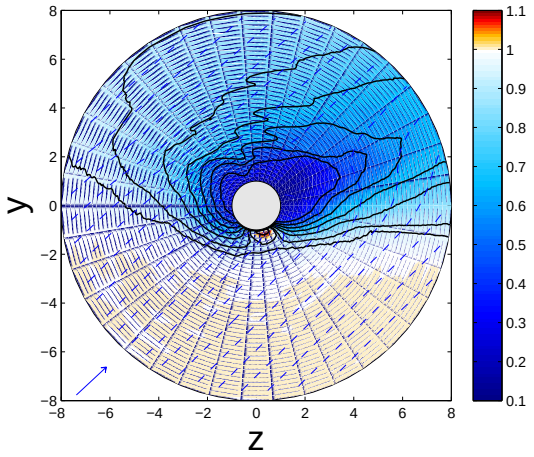

(d) $\lambda_{De} = 1$

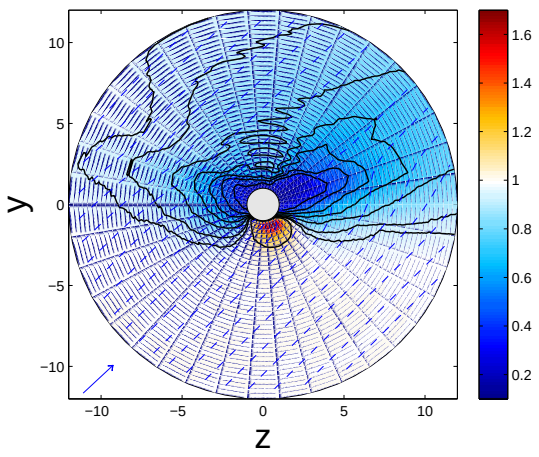

Figure 4: Selection of ion charge-density contour-plots in the $\{0, \mathbf{e_y}, \mathbf{e_z}\}$-plane, with magnetization $\beta_i = 5$ for $\tau = 1$, $v_d = c_{s0}$, $\delta = \pi/4$, $\phi_p = -8$, and different electron Debye lengths. Iso-density contours for $n_i = 0.4, 0.5, 0.6, 0.7, 0.8, 0.9, 0.95, 1.1$ are shown in solid black, while fluid stream-lines are shown in dashed blue. The external velocity is indicated by a blue arrow on the figures' lower left corners.

3.2 Strong ion magnetization with finite Debye length

Running SCEPTIC3D with $\lambda_{De} \lesssim 0.03$ is hardly practical because of the excessive number of radial cells required, yet we also need to explore the entire range R_L/Λ_{De}. We therefore use a moderately large $\beta_i = 5$, i.e. an average external ion Larmor radius equal to a fifth of probe radius, to study the strongly magnetized limit. Figure (4) shows a selection of ion charge-density contour-plots computed by SCEPTIC3D in the $\{0, \mathbf{e_y}, \mathbf{e_z}\}$-plane for $\beta_i = 5$; the electron Debye length is increased from $\lambda_{De} = 0.03$ to $\lambda_{De} = 1$ while the other parameters are kept fixed ($\tau = 1$, $v_d = c_{s0}$, $\delta = \pi/4$ and $\phi_p = -8$).

Figures (4a,b), computed with $\lambda_{De} = 0.03$ and $\lambda_{De} = 0.1$, are qualitatively similar to each other and to the quasineutral contour-plots discussed in Ref. [1]. Although the $\{0, \mathbf{e_y}, \mathbf{e_z}\}$-plane is shown, other parallel planes (approximately) have the same density distribution (Recall that in the strongly magnetized, quasineutral limit, planes of flow and field are independent, see Fig. (13).). The property demonstrated in that same limit that in the probe magnetic shadow (cylinder of radius R_p centered on the probe and parallel to $\mathbf{B}$) density contour-lines are straight and tangent to the probe surface [14, 13] approximately holds, although the leading edge perturbation front extends further with finite Debye length and ion Larmor radius. Also shown are fluid stream-lines, drawn from the fluid velocity $\langle \mathbf{v} \rangle$ that SCEPTIC3D outputs by averaging the computational ions' velocities in each computational cell.

Profiles in Figs (4c,d), computed with $\lambda_{De} = 0.3$ and $\lambda_{De} = 1$, are significantly different. In particular the contour-lines are not tangent to the collector, and an ion accumulation point forms at the probe leading edge. The transition occurs between $\lambda_{De} = 0.1$ and $\lambda_{De} = 0.3$, i.e. when the electron Debye length approximately equals the external average ion Larmor radius (from region X1 to X2 in Fig. (1)). The accumulation point is due to ions whose cross-field velocity v_y has been reduced from $v_\perp$ by the shielded convective electric field.

The regime transition at $\Lambda_{De} \simeq R_L$ is perhaps even clearer in Fig. (5), where ion charge-density contour-plots for the same parameters ($\beta_i = 5$, $\tau = 1$, $v_d = c_{s0}$, $\delta = \pi/4$, $\phi_p = -8$) are plotted in the $\{0, \mathbf{e_x}, \mathbf{e_y}\}$-plane (that is, looking along $-\mathbf{B}$) for (a) $\lambda_{De} = 0.1$ and (b) $\lambda_{De} = 0.3$. While $R_L \gtrsim \Lambda_{De}$, the ion cross-field velocity is approximately constant and given by $\mathbf{v}_\perp$; the picture according to which each slice in the plane of flow and magnetic field is independent of each other still (approximately) holds. When $R_L \lesssim \Lambda_{De}$ on the contrary, the probe negative bias permeates far enough in the plasma region to displace the magnetic presheath.

3.3 Intermediate ion magnetization

Figure (6) shows ion charge-density contour-plots computed by SCEPTIC3D at the intermediate magnetization $\beta_i = 1$, with $\tau = 0.1$, $v_d = 0.35 c_{s0}$, $\delta = \pi/2$, $\phi_p = -8$ and (a),(b) $\lambda_{De} = 0.3$, (c),(d) $\lambda_{De} = 3$.

Although the contour-lines in Fig. (6a) are not tangent to the probe surface due to the non-negligible electron Debye length, they are qualitatively similar to what was observed in Figs (4a,b), taking into account the fact that the drift velocity is different. Figure (6c) on the contrary reminds us of Figs (4c,d), with the leading-edge accumulation point. The transition occurs between $\lambda_{De} = 0.3$ and $\lambda_{De} = 3$, i.e. when $\Lambda_{De} \simeq R_L$ as expected.

Figure (6c) also shows an accumulation point in the trailing edge, absent in Figs (4c,d) because the drift velocity was too high. Both the leading and trailing edge accumulation points correspond to regions where the convective electric field is shielded enough for the ions to have negligible

(a) $\lambda_{De} = 0.1$ (b) $\lambda_{De} = 0.3$

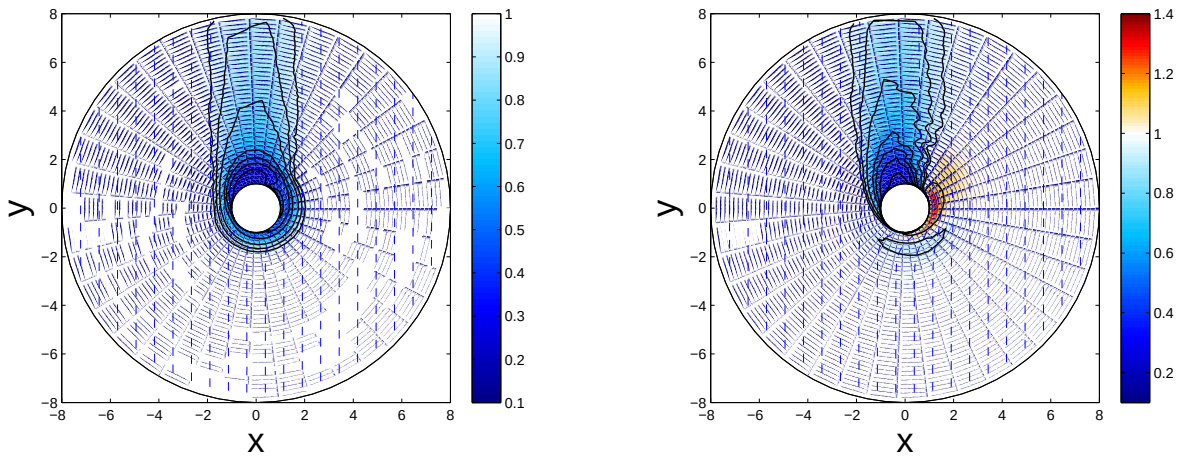

Figure 5: Selection of ion charge-density contour-plots in the $\{0, \mathbf{e_x}, \mathbf{e_y}\}$-plane, with magnetization $\beta_i = 5$ for $\tau = 1$, $v_d = c_{s0}$, $\delta = \pi/4$, $\phi_p = -8$ and (a) $\lambda_{De} = 0.1$, i.e. $\lambda_{De} < r_L$, (b) $\lambda_{De} = 0.3$, i.e. $\lambda_{De} > r_L$. Iso-density contours for $n_i = 0.4, 0.5, 0.6, 0.7, 0.8, 0.9, 0.95, 1.1$ are shown in solid black, while fluid stream-lines are shown in dashed blue.

cross-field velocity. They perform "mirror oscillations" along the field lines in the probe-induced potential well, as illustrated in Fig. (3a) by the orbit labeled "$w_o = -5.16$". Because arising in a region of weakened convective electric field, those oscillations can also occur in stationary plasmas, as discussed in Ref. [5]. An interesting question that could be addressed in future work is the importance of trapped ions in this case.

Figure (6b,d) shows ion density-contours in the $\{0, \mathbf{e_x}, \mathbf{e_y}\}$-plane, computed using the same parameters as in Fig. (6a,c). As first observed in Fig. (5), the fluid stream-lines belonging to the cross-field plane start to encircle the probe when $\Lambda_{De} \gtrsim R_L$. It is interesting to parallel those stream-lines with the ion orbits shown in Fig. (3a). Figure (6d) is qualitatively comparable to Fig. (11) in Ref. [24], which shows magnetized electron orbits encircling a positively charged probe in the vacuum limit.

3.4 Electrostatic potential distribution

Figure (7) shows electrostatic potential (ϕ) contour-lines for $\lambda_{De} = 0.1$ and $\lambda_{De} = 3$, using the same parameters as in Figs (4,5). It can be seen that when $\Lambda_{De} \ll R_p$, the contours are well coupled to the ion density distribution (compare Figs (7a,b) with Figs (4b,5a)). Because Poisson's equation smoothes out density gradients over a scale length Λ_{De}, the potential contours when $\Lambda_{De} \gtrsim R_p$ tend to a more circular form in the $\{0, \mathbf{e_y}, \mathbf{e_z}\}$-plane. In the $\{0, \mathbf{e_x}, \mathbf{e_y}\}$-plane (Fig. (7d)), the contours in the probe vicinity are shifted in the positive x direction, due to the effective probe dipole permeating in the plasma region.

(a) $\lambda_{De} = 0.3$

(b) $\lambda_{De} = 0.3$

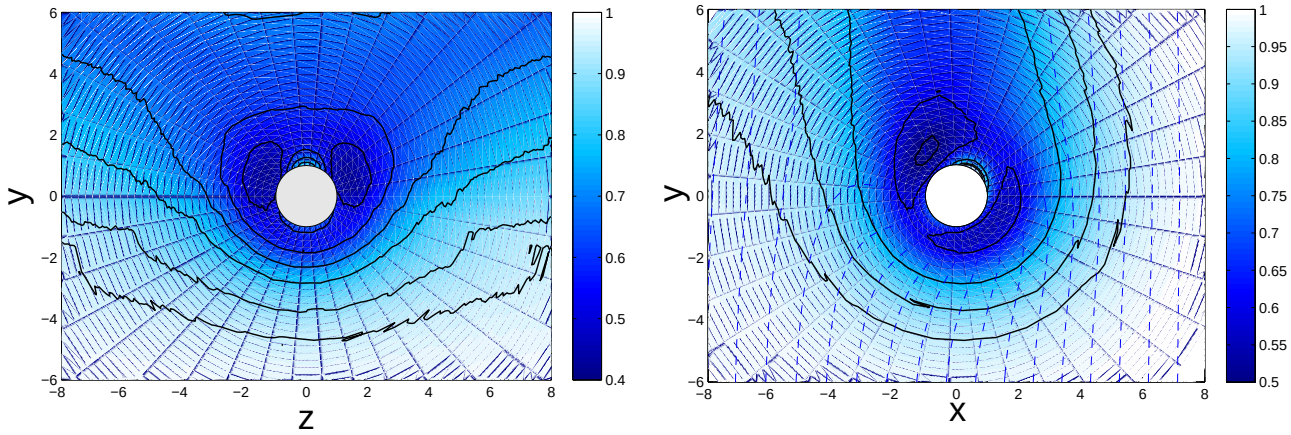

(c) $\lambda_{De} = 3$

(d) $\lambda_{De} = 3$

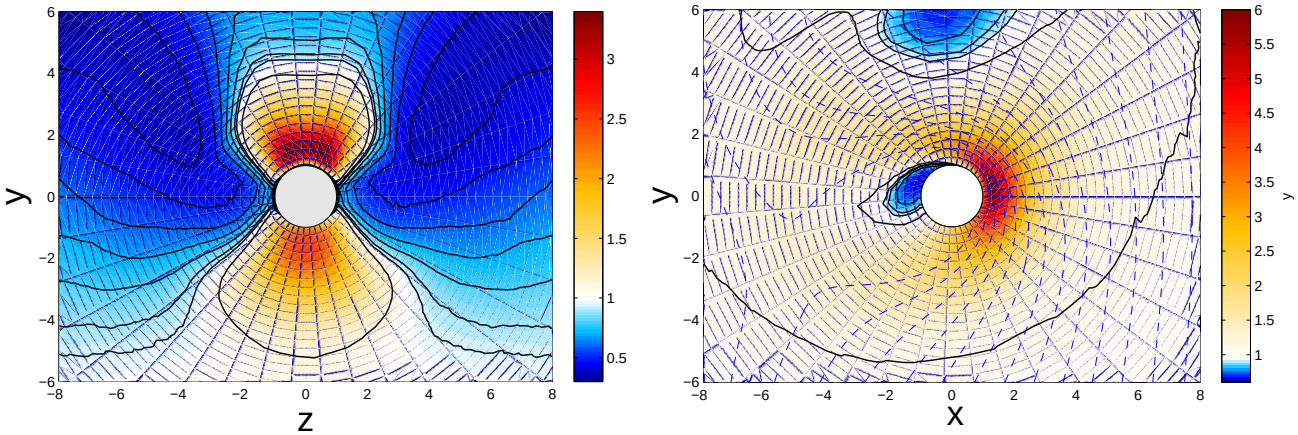

Figure 6: Ion charge-density contour-plots with magnetization $\beta_i = 1$ for $\tau = 0.1$, $v_d = 0.35 c_{s0}$, $\delta = \pi/2$, $\phi_p = -8$ in the (a) $\{0, \mathbf{e_y}, \mathbf{e_z}\}$-plane for $\lambda_{De} = 0.3$, (b) $\{0, \mathbf{e_x}, \mathbf{e_y}\}$-plane for $\lambda_{De} = 0.3$, (c) $\{0, \mathbf{e_y}, \mathbf{e_z}\}$-plane for $\lambda_{De} = 3$, (d) $\{0, \mathbf{e_x}, \mathbf{e_y}\}$-plane for $\lambda_{De} = 3$. Fluid stream-lines in (b,d) are shown in dashed blue

(a) $\{0, \mathbf{e_y}, \mathbf{e_z}\}$, $\lambda_{De} = 0.1$

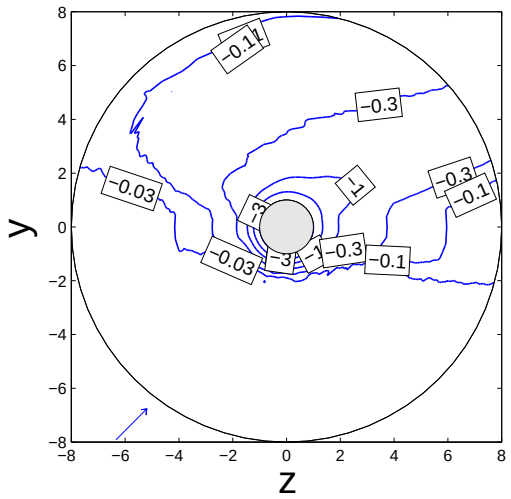

(b) $\{0, \mathbf{e_x}, \mathbf{e_y}\}$, $\lambda_{De} = 0.1$

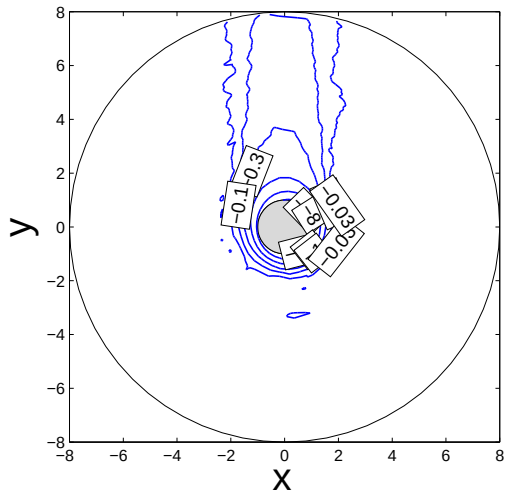

(c) $\{0, \mathbf{e_y}, \mathbf{e_z}\}$, $\lambda_{De} = 3$

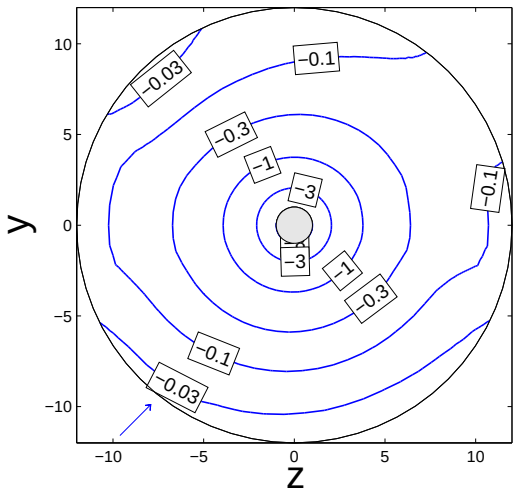

(d) $\{0, \mathbf{e_x}, \mathbf{e_y}\}$, $\lambda_{De} = 3$

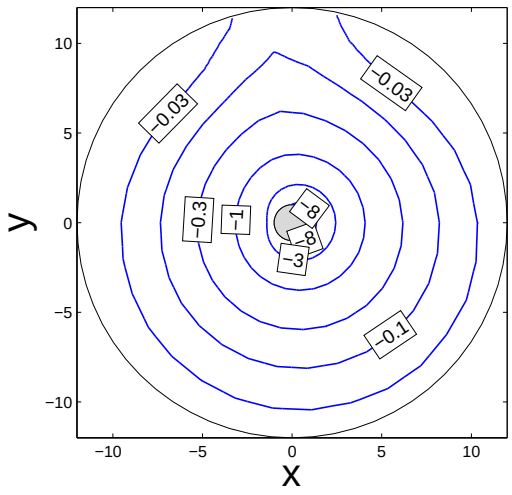

Figure 7: Potential (ϕ) contour-lines with magnetization $\beta_i = 5$ for $\tau = 1$, $v_d = c_{s0}$, $\delta = \pi/4$, $\phi_p = -8$ in the (a) $\{0, \mathbf{e_y}, \mathbf{e_z}\}$-plane for $\lambda_{De} = 0.1$, (b) $\{0, \mathbf{e_x}, \mathbf{e_y}\}$-plane for $\lambda_{De} = 0.1$, (c) $\{0, \mathbf{e_y}, \mathbf{e_z}\}$-plane for $\lambda_{De} = 3$, (d) $\{0, \mathbf{e_x}, \mathbf{e_y}\}$-plane for $\lambda_{De} = 3$. The external velocity is indicated by a blue arrow on the figures' lower left corners.

3.5 Wakefields

Looking further away from the probe, where the potential is weak and the plasma dynamics is linear, we expect to observe ion cyclotron wakes whose wave-length is given by

$$\Lambda_{\rm Wake} = 2\pi\frac{v_\perp}{\omega_c} = 4\sqrt{\pi}R_p\frac{w_\perp}{\beta_i}. \tag{18}$$

Figure (8a) shows the ion charge-density colour-plot in the $\{0, \mathbf{e_x}, \mathbf{e_y}\}$-plane computed by SCEPTIC3D for $\tau = 1$, $\phi_p = -8$, $v_d = c_{s0}$, $\delta = \pi/2$, $\lambda_{De} = 10$ and $\beta_i = 0.5$. The cyclotron wake is clearly visible, and has a wavelength matching the theoretical formula (18) within less than 2% for the first two minima, and 1% afterwards. The wakefield is parallel to $\mathbf{v}_\perp$, but slightly displaced, to $x \simeq -1$. The wake is insensitive to the Debye length, provided it is large enough, approximately $\lambda_{De} \gtrsim 3$. Below this limit, cyclotron damping (proportional to the plasma frequency squared, hence to λ_{De}^{-2}) appears to be too strong. For example in Fig. (6d) the first minimum of the wakefield is visible at $y \simeq 5.55R_p$ ($\lambda_{De} = 3$), but not in Fig. (6b) where $\lambda_{De} = 0.3$.

(a) $\tau = 1$, $\lambda_{De} = 10$ (b) $\tau = 0.1$, $\lambda_{De} = 20$

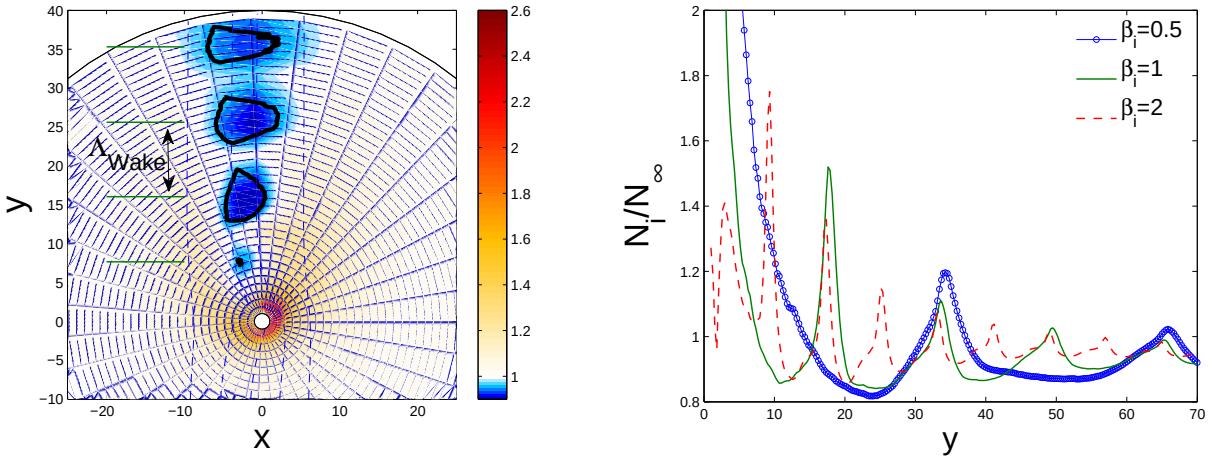

Figure 8: (a) Ion charge-density colour-plot in the $\{0, \mathbf{e_x}, \mathbf{e_y}\}$-plane, for $\tau = 1$, $\phi_p = -8$, $v_d = c_{s0}$, $\delta = \pi/2$, $\lambda_{De} = 10$ and $\beta_i = 0.5$. The depletion minima of the wakefield are indicated by thick black contour-lines at $N_i/N_\infty = 0.95$. (b) Ion charge-density at $z = 0$ and $x = -1$ as a function of y, for $\tau = 0.1$, $\phi_p = -8$, $v_d = c_{s0}$, $\delta = \pi/2$, $\lambda_{De} = 20$, and different ion magnetization levels.

Reducing the ion temperature increases the intensity of the wakefield, since the probe potential in ion thermal units $\chi_p = -\phi_p/\tau$, responsible for the "kick" launching the wake, increases. Figure (8b) is a plot of wake ion charge-density versus cross-field position at $x = -1$ and $z = 0$ for $\tau = 0.1$, $\phi_p = -8$, $v_d = c_{s0}$, $\delta = \pi/2$, $\lambda_{De} = 20$ and three levels of magnetization ($\beta_i = 0.5, 1, 2$). In the considered conditions ($w_\perp \simeq 2.23$), Eq. (18) predicts $\Lambda_{\rm Wake} = \{31.7, 15.9, 7.9\}R_p$, which match SCEPTIC3D computations to within 1%, i.e. about the uncertainty in plot reading.

4 Ion current

4.1 Transverse velocity effects in asymptotic regimes

We start our analysis of current collection by studying transverse velocity effects in the strongly magnetized vacuum limit (region 7), with the drift approach presented in section 3.1.2; the total ion current I_i is therefore obtained by summing the flux-density $\Gamma_{i\parallel}$ (Eq. (17)) over the entire sphere surface.

The solution is plotted in Fig. (9a) as a function of cross-field drift $w_\perp$ for a selection of probe potentials χ_p, with no external parallel drift ($w_\infty = 0$), i.e. $w_d = w_\perp$. In the limit $w_\perp \to 0$, the ion current tends to the geometric limit $I_i = I_i^0/2$ regardless of χ_p, because only ions from the probe magnetic shadow can be collected. The rapid increase in current with $w_\perp > 0$ is caused by cross-field repopulation of the magnetic shadow, not by direct drift flux to the upstream surface (since all probe-surface-flux is parallel in the drift approximation). With drift velocity of order the ion-thermal velocity, large enhancements of the flux above the ballistic asymptote given by $I_i = \pi R_p^2 N_\infty w_d v_{ti}$, are observed. But for large enough drifts, the ion current eventually falls below the ballistic value.

(a) Drift model (b) OML

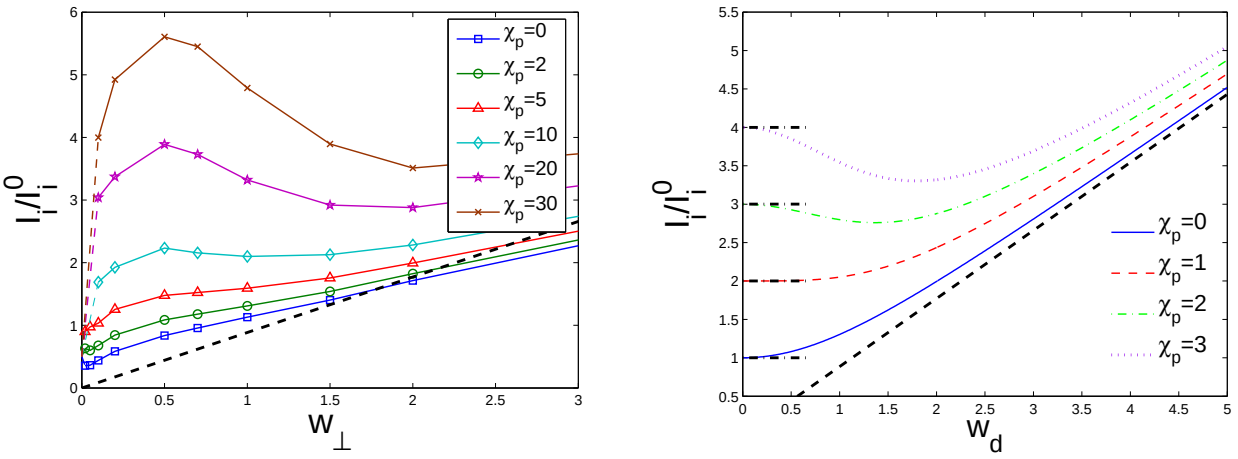

Figure 9: Total ion current normalized to $I_i^0 = 4\pi R_p^2 N_\infty v_{ti}/2\sqrt{\pi}$. (a) From the strongly magnetized drift calculations of section 3.1.2 with $\beta_i = 100$ and $w_\infty = 0$, and (b) from the unmagnetized OML model. The thick dashed lines correspond to the ballistic asymptote, and horizontal dash-dotted lines in (b) to the stationary OML limit. In (a), the currents at $w_\perp = 0$ (i.e. $I_i/I_i^0 = 1/2$) cannot be computed from our drift model because of a singularity in the equations; this is signified by dashed portions of curves for $w_\perp$ below the first computed values.

Figure (9b) is the counterpart of Fig. (9a) in the opposite limit of zero ion magnetization, yet $\Lambda_{De} \gg R_p$ (region 1). In such conditions there is no convective electric field nor intermediate effective potential barriers. Each ion whose energy and angular momentum at infinity is compatible with collection is therefore collected, and the current becomes the Orbit Motion Limited (OML)

value [3, 9]

$$I_i = I_i^0 \left[\frac{1}{2} \exp\left(-w_d^2\right) + \frac{\sqrt{\pi}}{2} \left(w_d + \frac{1}{2w_d} + \frac{\chi_p}{w_d} \right) \mathrm{erf}\left(w_d\right) \right]. \tag{19}$$

Unmagnetized currents do not tend to a fixed low value at $w_d \to 0$, and show minima rather than maxima at intermediate w_d.

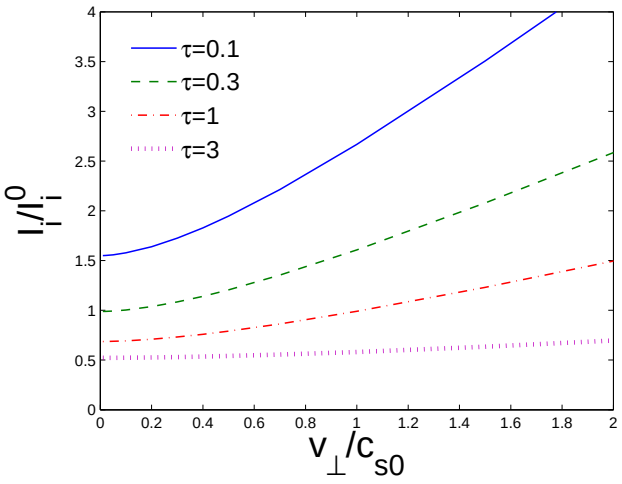

Figure 10: Total (i.e. sphere-integrated) ion current normalized to $I_i^0 = 4\pi R_p^2 N_\infty v_{ti}/2\sqrt{\pi}$, solution of the collisionless quasineutral 1D-kinetic model of Ref. [13], valid when $(\Lambda_{De}, R_L) \ll R_p$, here with $v_\infty = 0$. Except in the limit $\tau \gg 1$, the ion current at $v_\perp = 0$ is higher than the geometric limit $I_i^0/2$.

The opposite limit, $\Lambda_{De} \to 0$, $R_L \to 0$ (region 5), is shown in Fig. (10). This collisionless quasineutral limit is obtained by sphere-integration of the ion flux-density at the sheath entrance computed with the method described in Ref. [13] (Eq. (17) in that same publication). The quasineutral current does not tend to the geometric limit $I_i = I_i^0/2$ when $v_\perp \to 0$, except if $\tau \gg 1$ when the only electric field "felt" by the ions is $\mathbf{E}_{\mathrm{conv}}$ (free-flight limit).

As explained in Refs [13, 14], no self-consistent solution to the collisionless strongly magnetized plasma equations exists in the absence of convective drift. As $v_\perp/c_{s0}$ becomes smaller, the collection region elongates until either collisions reduce the current below the "zero-drift" value of Fig. (10) or else diffusive cross-field transport in the magnetic shadow starts to dominate. Only the free-flight and the vacuum limits allow a rigorous collisionless treatment of the stationary magnetized probe problem, because ions and electrons are then decoupled. The vacuum limit problem at arbitrary magnetization without drift was first studied by Sonmor and Laframboise [12]. Reference [5] was focussed on collisionless ion collection by spherical probes in stationary magnetoplasmas, and only weak enough magnetic fields ($\beta_i \lesssim 1$) could be considered in order to ensure physically meaningful results.

4.2 Finite magnetization and Debye length effects

Figure (11) shows the total ion current dependence on ion magnetization β_i for a selection of transverse drift velocities and electron Debye lengths, with probe potential $\phi_p = -8$ and temperature ratio $\tau = 1$, self-consistently computed with SCEPTIC3D.

(a) $v_d = 0.2c_{s0}$

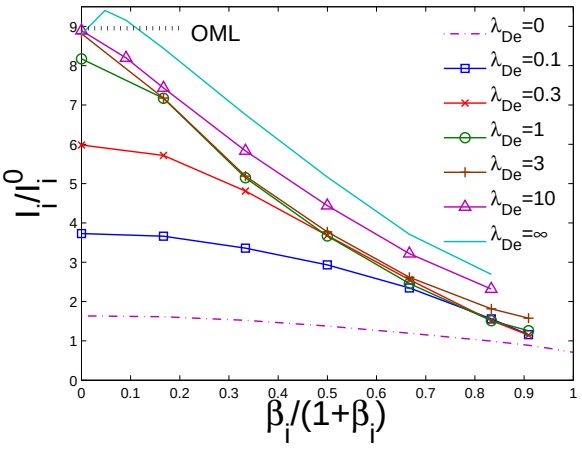

(b) $v_d = 0.5c_{s0}$

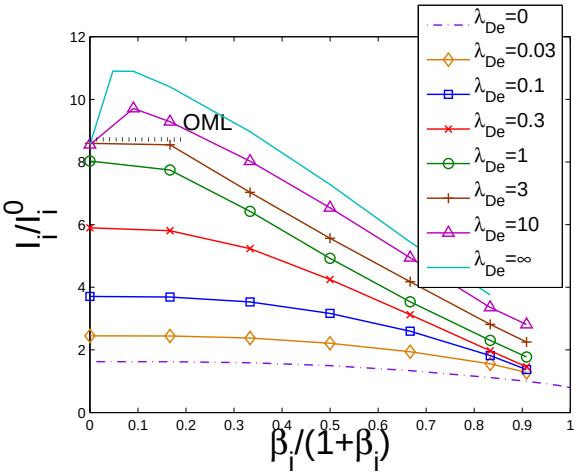

(c) $v_d = c_{s0}$

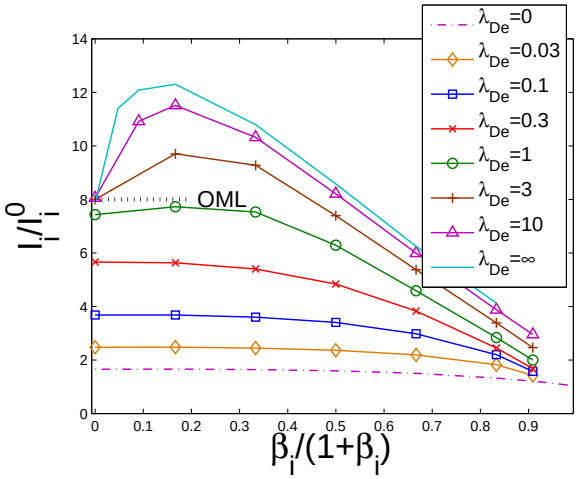

(d) $v_d = 1.5c_{s0}$

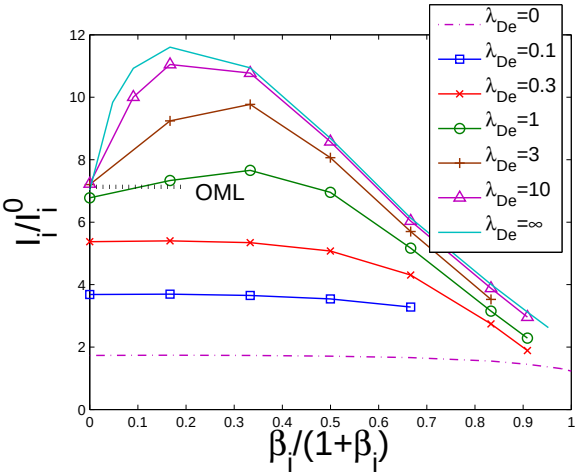

Figure 11: Total ion current normalized to $I_i^0 = 4\pi R_p^2 N_\infty v_{ti}/2\sqrt{\pi}$ as a function of ion magnetization β_i, self-consistently calculated with SCEPTIC3D with $\tau = 1$, $\phi_p = -8$ and $\delta = \pi/2$. Curves labeled "$\lambda_{De} = 0$" refer to quasineutral computations [1], and curves labeled "$\lambda_{De} = \infty$" to calculations performed with $\lambda_{De} = 70$. (a) $v_d = 0.2c_{s0}$. (b) $v_d = 0.5c_{s0}$. (c) $v_d = c_{s0}$. (d) $v_d = 1.5c_{s0}$.

We first see that curves of current versus magnetization at $\lambda_{De} = 0$ and $\lambda_{De} = \infty$ form envelopes for the corresponding curves at intermediate shielding. In the absence of magnetic field

and in the limit $\Lambda_{De} \gg R_p$ (region 1), the ion current approaches the Orbit Motion Limited (OML) value (19). As the Debye length is shortened, the extent of the potential perturbation is reduced and the effective collection radius decreases; as a consequence the ion current reduces as well, down to the quasineutral limit where it becomes independent of the probe bias [2, 7].

Under magnetized conditions, however, the current is not necessarily a monotonic function of λ_{De}. It was shown in Ref. [5] that in *stationary* weakly magnetized plasmas, the current would peak at intermediate Debye lengths. What Fig. (11) shows is that provided there is a transverse drift ($0.2c_s$ is sufficient) the current does increase monotonically with λ_{De}.

A second important result from Fig. (11) is that in the presence of cross-field drift, the total ion current can exceed the unmagnetized value at low but non-zero magnetic field. We can see here that the faster the cross-field flow, the lower the Debye length threshold at which this peak occurs. A further observation is that when the peak is present, its maximum is located at a magnetization level increasing with decreasing Debye length. Although it is hard to propose a ready-to-use formula predicting the location and height of those maxima, the location qualitatively *scales* as $R_p/v_\perp = O\left(1/\omega_c\right)$ ($\beta_i = O\left(w_\perp\right)$), i.e. the maximum occurs when the transverse ion transit time compares to the Larmor period.

This effect was already noticed in previous quasineutral computations [1], although it was much less pronounced. The physical origin is nevertheless the same. When $\beta_i = 0$, the probe focusses the ions downstream; as β_i increases, part of the ions that would miss the probe in the absence of magnetic field are collected downstream while the upstream current is unaffected. Perhaps an easier way to understand this phenomenon is to look at the critical stream-lines in the $\{0, \mathbf{e_y}, \mathbf{e_z}\}$-plane at $\beta_i = 0$ and $\beta_i = 0.1$, shown in Fig. (12) for infinite λ_{De}, $\chi_p = 15$, $w_\perp = 0.5$ and $w_\infty = 0$. The collection flux-tube, meaning the volume made of all the collected stream-lines, is broader for weak but non-zero magnetic field. In the absence of transverse drift, this phenomenon cannot happen and the current *must* decrease with increasing β_i (The decrease is in fact linear in β_i at low β_i [5].).

The ion current in Fig. (11) seems to have a $1/\beta_i$ dependence at high β_i, which is consistent with observations made in the quasineutral regime [1]. This is because we limit our simulations to values of β_i such that no part of the probe is ion-repelling (to be rigorous, points at $\beta_i = 10$ in Figs (11c,d) should be excluded). Further increasing β_i would lead to part of the probe being ion-repelling (thus invalidating our Boltzmann electrons model), but the other part much more ion-attracting.

5 Transverse Mach probe calibration

We have so far parameterized the probe surface using the angles θ and ψ, a subset of SCEPTIC3D's spherical coordinate system (r, θ, ψ) (see Fig. (2)). Following the analysis of Refs [1, 13] however, Mach probe surfaces are most conveniently parameterized by x and η, where η is the angle between the magnetic field and the probe tangent in the plane of field and drift[1]. The geometry is illustrated in Fig. (13); only on the probe major cross-section ($x = 0$ or $\psi = \pm\pi/2$) does θ correspond to η, although shifted by $\pi/2$.

As discussed in the introduction, Mach probes operate by measuring ion flux-densities Γ_i in different directions, the asymmetry of which is then used to deduce the unperturbed plasma velocity. In theory Mach probes work if $\Lambda_{De} \lesssim R_L$ so that the ions do not see the probe shielding of the convective electric field, and $\Lambda_{De} \lesssim R_p$ in order for orbital effects not to "shuffle" information about

[1]The angle θ in Ref. [14] corresponds to η in Refs [1, 13] and in the present publication.

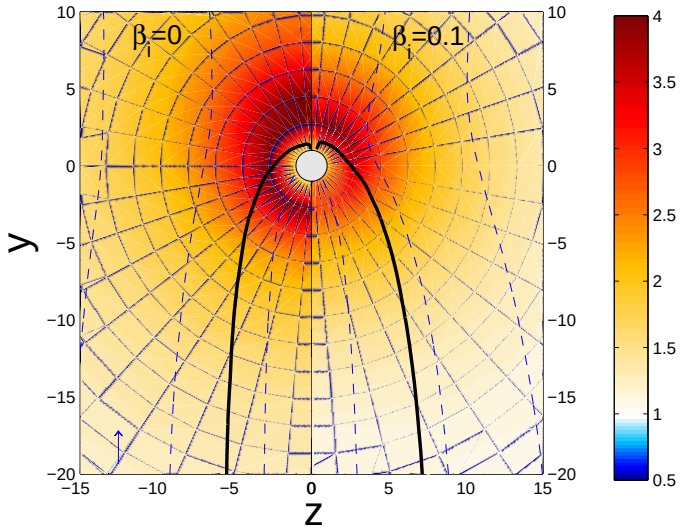

Figure 12: Normalized ion charge-density colour-plots in the $\{0, \mathbf{e_y}, \mathbf{e_z}\}$-plane with (left) zero and (right) weak magnetization $\beta_i = 0.1$. The Debye length is infinite, hence the temperature ratio τ irrelevant. The probe bias is $\chi_p = 15$, and the external drift velocity is $w_\perp = 0.5$ and $w_\infty = 0$. The thick black lines are the critical stream-lines delimiting the collection flux-tube, while other stream-lines are shown in dashed blue.

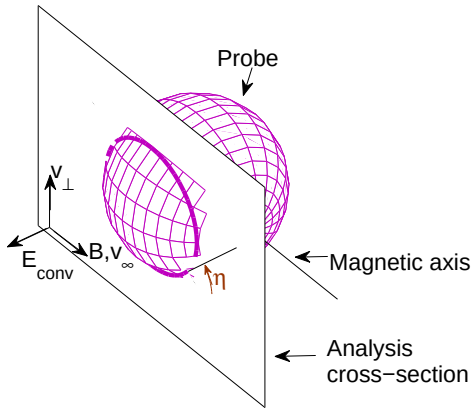

Figure 13: Geometry of the spherical Mach probe problem. In the quasineutral strongly magnetized limit ($(\Lambda_{De}, R_L) \ll R_p$, i.e. region 5), planes of magnetic field and drift are independent. η is defined as the angle between the magnetic field and the probe tangent in such a plane. From Ref. [1].

the external velocity. This was the parameter regime explored in Ref. [1], a major result of which was that 4-pin transverse Mach probes, with collector surfaces at $\eta = \pm\pi/4$ and $\eta = \pm 3\pi/4$ to the magnetic field in a plane of flow and magnetic field, give the velocities from two flux ratios, denoted $R_{3\pi/4} \equiv \Gamma_i(\eta = -\pi/4)/\Gamma_i(\eta = 3\pi/4)$ and $R_{\pi/4} \equiv \Gamma_i(\eta = -3\pi/4)/\Gamma_i(\eta = \pi/4)$. On the sphere *major cross-section*, those measurement points correspond to normals at angles (θ) of 45 degrees to the magnetic field ($\cos\theta = \pm 1/\sqrt{2}$, $\sin\theta = \pm 1/\sqrt{2}$).

The flow (in terms of a Mach number M that we define as velocity normalized by the isothermal ion sound speed c_{sI}, see Eq. (4)) could be calibrated with a single factor M_c, function of β_i and τ only, and deduced from

$$M_\perp = \frac{M_c}{2}\left(\ln R_{3\pi/4} - \ln R_{\pi/4}\right) \tag{20}$$

$$M_\infty = \frac{M_c}{2}\left(\ln R_{3\pi/4} + \ln R_{\pi/4}\right). \tag{21}$$

Flux-sensing probes rarely operate in the simultaneous limit $\Lambda_{De} \gg R_p$ and $R_p \gg R_L$ (region 7). It is nevertheless instructive to start our investigation of finite Debye length effects from there. Figure (14a) shows the ion flux-density to the probe major cross-section in the plane of flow and magnetic field $\{0, \mathbf{e_y}, \mathbf{e_z}\}$ as a function of $\cos\theta$. The curves are therefore closed on themselves, the upper portions corresponding to $\sin\theta \leq 0$ (upstream) and the lower portions to $\sin\theta \geq 0$ (downstream). The conditions are an infinite Debye length (hence τ is irrelevant), $w_\perp = 0.5$, $w_\infty = 0$, and $\chi_p = 50$. The dotted curve, referring to the drift solution of section 3.1.2, vanishes on the probe leading edge ($\theta = -\pi/2$) in addition to vanishing on the trailing edge ($\theta = \pi/2$). We also show SCEPTIC3D's computed fluxes, never exactly vanishing because finite ion magnetization tends to smooth discontinuities. Elsewhere, this effect is absent and SCEPTIC3D agrees quite well with the drift approximation. The observation that in the limit of vanishing Larmor radius no current is collected on the $\{0, \mathbf{e_x}, \mathbf{e_y}\}$-plane was already made in Ref. [24] in the context of electron collection by positively charged spacecraft.

Figure (14b) shows flux ratios as a function of $w_\perp$ when $w_\infty = 0$, and $\Lambda_{De} \gg R_p$, in the drift approximation. The ratios tend to unity at $w_\perp = 0$, but do not increase exponentially (or even monotonically) with $w_\perp$ as is the case in quasineutral plasmas (Eqs (20,21)). For strong enough cross-field drift, the flux ratio becomes less than 1, which is reminiscent of a similar asymmetry reversal observed in the magnetic-free regime [3]. Another interesting feature of Fig. (14b) is the presence of two flux-ratio maxima at large χ_p, for which we do not have a simple physical explanation. The non-monotonic relationship between flux ratios and drift velocity makes it difficult to imagine a Mach-probe being able to measure velocity in this long-Debye length regime.

When the Debye length is smaller than the probe radius, however, deducing velocity becomes feasible. Figure (15) shows scatter plots of the ratios $R_{3\pi/4}$ and $1/R_{\pi/4}$ on the probe major cross-section, computed by SCEPTIC3D for $\tau = 1$, $\phi_p = -8$, $\lambda_{De} = 0.1$ and various v_d and δ. They give reasonably straight lines in log-space against $M_\perp + M_\infty$ and $M_\perp - M_\infty$.

From a whole range of such plots, the calibration factors M_c in the ion magnetization range $\beta_i \in [0:10]$ for $\tau = 1$ and $\phi_p = -8$, are computed by fitting SCEPTIC3D's solutions for $v_d \lesssim c_{sI}$ and $\delta \in [\pi/8 : \pi/2]$ (M_c is the inverse of the fitting lines' slopes.). The results are plotted in Fig. (16) on (a) the major cross-section ($x = 0$) and (b) the quarter cross-sections ($x = \pm 1/\sqrt{3}$). Figure (16a) also shows the fitting error bars, whose widths for each value of β_i and λ_{De} are equal to twice the standard deviation of the respective scatter plots (such as shown in Fig. (15)) about their fitting line.

(a) (b)

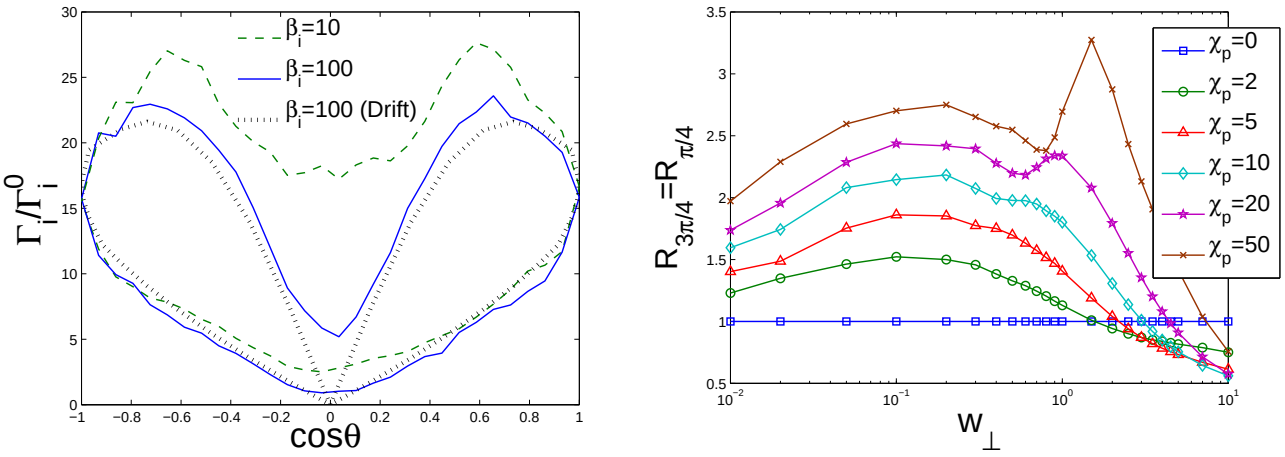

Figure 14: (a) Angular ion flux-density distribution to the probe major cross-section in the plane of flow and magnetic field $\{0, \mathbf{e_y}, \mathbf{e_z}\}$ normalized to $\Gamma_i^0 = N_\infty v_{ti}/(2\sqrt{\pi})$, with probe bias $\chi_p = 50$. Calculations have been performed with SCEPTIC3D in a vacuum potential (i.e. infinite Debye length) for $\beta_i = 10$ and $\beta_i = 100$, with $w_\perp = 0.5$ and $w_\infty = 0$. "Drift" refers to the drift calculations of section 3.1.2 with $\beta_i = 100$. (b) Flux ratios $R_{3\pi/4} = R_{\pi/4}$ as a function of $w_\perp$ with $w_\infty = 0$, obtained with the drift model for $\beta_i = 100$.

(a) (b)

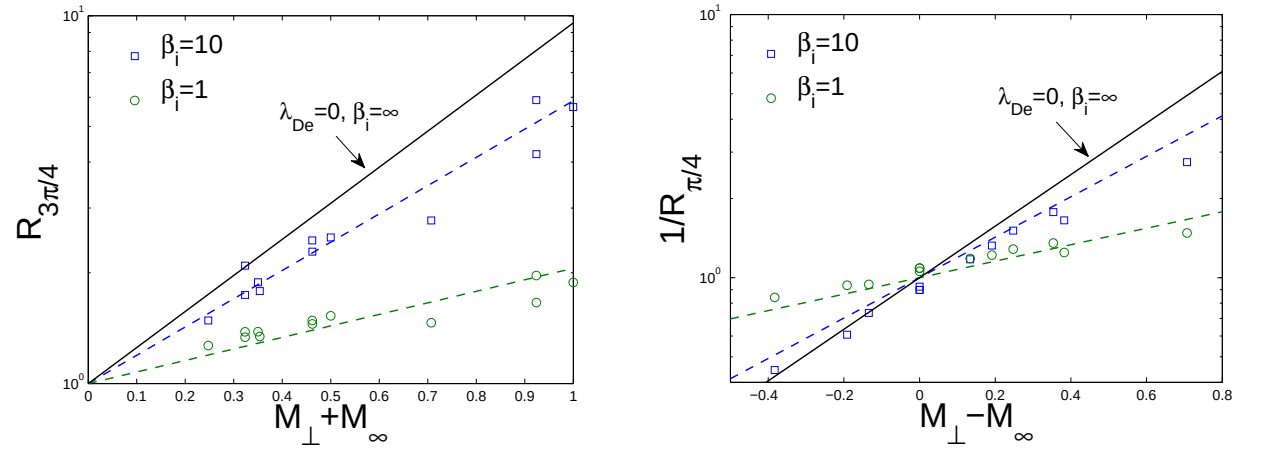

Figure 15: Upstream to downstream flux 45-degree ratios on the probe major cross-section, versus respectively $M_\perp + M_\infty$ and $M_\perp - M_\infty$, from a large set of SCEPTIC3D runs spanning $v_d \in [0:1]c_{s0}$ and $\delta \in [\pi/8 : \pi/2]$, for $\tau = 1$, $\lambda_{De} = 0.1$, and $\phi_p = -8$. Also shown are the corresponding fitting lines (dashed), whose slopes $1/M_c$ correspond to points in Fig. (16). The solid line is the strongly magnetized quasineutral result for $\tau = 1$ from Ref. [13].

(a) Major cross-section (b) Quarter cross-sections

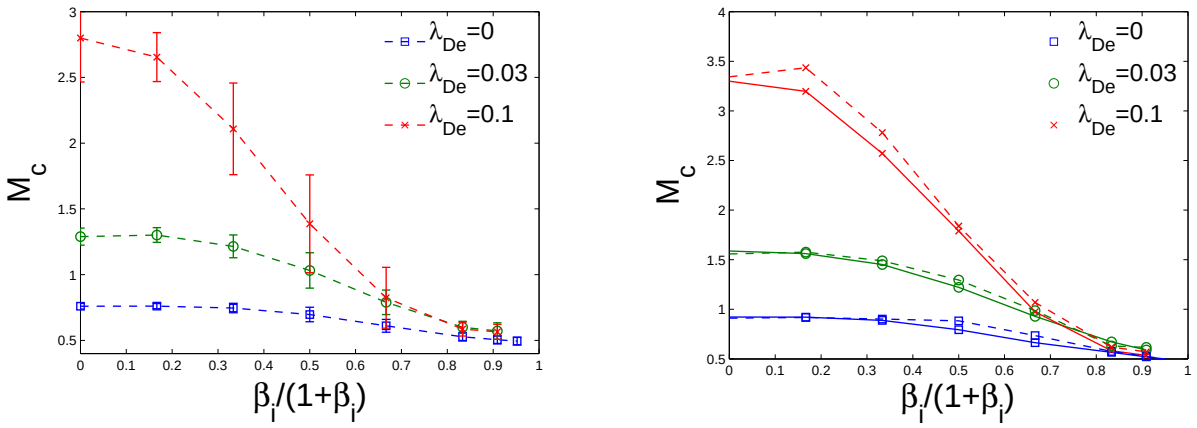

Figure 16: Transverse Mach probe calibration factor M_c as a function of ion magnetization β_i and electron Debye length λ_{De} for $\tau = 1$ and $\phi_p = -8$, computed with SCEPTIC3D for measurements made (a) on the major cross-section and (b) the quarter cross-sections. (a) also shows the fitting error bars, mostly arising from Eqs (20,21) being only approximate. On (b), solid lines refer to measurements at $x = 1/\sqrt{3}$, and dashed lines to measurements at $x = -1/\sqrt{3}$. Curves labeled "$\lambda_{De} = 0$" are taken from Fig. (14) in Ref. [1].

The width of those error bars, or equivalently the quality of the fittings shown in Fig. (15), can mostly be explained by Eqs (20,21) being only approximate. Numerical noise (e.g. statistical noise due to the use of an insufficient number of computational ions, biases from unconverged runs, ...) only plays a marginal role here because extreme care has been taken in the selection of computational parameters; this is confirmed by the the error bars being very short for large β_i and $\lambda_{De} = 0$ where the fitting (20,21) is exact [13].

Error bars have not been plotted on Fig. (16b) to increase readability, but are qualitatively similar to those in Fig. (16a). At intermediate magnetization, Mach probes with electrodes whose normals are not on the major cross-section are sensitive to the magnetic field orientation. This phenomenon, already observed in the "$\lambda_{De} = 0$" limit [1], is due to finite Larmor radius effects. The flux ratios are lower at $x = -1/\sqrt{3}$ than $x = 1/\sqrt{3}$.

The fitting error bars get larger as the Debye length increases, indicating that the fitting (20,21) becomes less and less satisfactory. Error bars for $\lambda_{De} \gtrsim 0.3$ being excessively large, we can qualitatively say that accurate calibration is limited to $\lambda_{De} \lesssim 0.1$. At strong magnetization, the calibration factor is not very sensitive to the Debye length provided it is below the just-defined bound, and using the quasineutral strongly magnetized value [13, 14] ($M_c \simeq 0.5$) should yield an error well below typical experimental uncertainties. In other words, it is not required that $\Lambda_{De} \ll R_L$, but $\Lambda_{De} \lesssim 0.1 R_p$, provided that also $R_L \lesssim 0.1 R_p$, for the calibration to approach the quasi-neutral value.

6 Summary

This publication provides the first quantitative description of ion collection by a spherical conducting object in the presence of a convective transverse drift, in the entire range of magnetization and Debye length. The computations are performed with the hybrid PIC code SCEPTIC3D, introduced in Ref. [1] for quasineutral studies but here operated with its Poisson solver. The problem has a total of six dimensionless parameters: ion magnetization β_i, electron Debye length λ_{De}, drift velocity and orientation v_d/c_{s0} and δ, median probe bias ϕ_p and temperature ratio τ. Each of those triggers has its own effect on the physics, that SCEPTIC3D can fully capture.

At intermediate to strong magnetization ($\beta_i \gtrsim 1$), we report an important transition in plasma structure when the Debye length goes over the ion Larmor radius. The ion "$\mathbf{E} \times \mathbf{B}$" velocity is modified in the probe neighborhood where the convective electric field is shielded. In particular, little current can be collected at $z = 0$, i.e. where the probe surface is tangent to the magnetic field lines.

When the Debye length is large enough, an important result is that the total collected current can go well above the OML limit (see Fig. (11)). This effect cannot be seen in stationary plasmas [5]; it is due to magnetic focussing towards the probe of ions which, in unmagnetized conditions, would just have been deflected. For typical sonic or subsonic flows, this occurs at rather weak magnetization ($\beta_i \lesssim 0.3$ for $\chi_p = -\phi_p/\tau = 8$).

The 4-pin Mach probe calibration method derived for quasineutral plasmas [1] (Eqs (20,21)) is shown to hold up to Debye lengths equal to about 10% of the probe radius. The corresponding calibration factors at $\tau = 1$ and increasing λ_{De} are plotted against ion magnetization in Fig. (16). When both the Debye length and the Larmor radius are small compared to the probe dimensions however, their ratio does not affect the collection pattern significantly. For Larmor radii and Debye lengths below a tenth of probe radius, using the quasineutral strongly magnetized value ($M_c \simeq 0.5$ [14, 13]) should yield an error well below typical experimental uncertainties.

Acknowledgments

Leonardo Patacchini was supported in part by NSF/DOE Grant No. DE-FG02-06ER54891. Most SCEPTIC3D calculations were performed on the MIT PSFC Parallel Opteron/Infiniband cluster Loki.

References

[1] L. Patacchini and I.H. Hutchinson, *Spherical probes at ion saturation in* $\mathbf{E} \times \mathbf{B}$ *fields*, Plasma Phys. Control. Fusion **52**, 035005 (2010).

[2] I.H. Hutchinson, *Ion collection by a sphere in a flowing plasma: 1. Quasineutral*, Plasma Phys. Control. Fusion **44**, 1953-1977 (2002).

[3] I.H. Hutchinson, *Ion collection by a sphere in a flowing plasma: 2. Non-zero Debye length*, Plasma Phys. Control. Fusion **45**, 1477-1500 (2003).

[4] L. Patacchini and I.H. Hutchinson *Angular distribution of current to a sphere in a flowing, weakly magnetized plasma with negligible Debye length*, Plasma Phys. Control. Fusion **49**, 1193-1208 (2007).

[5] L. Patacchini and I.H. Hutchinson *Ion-collecting sphere in a stationary, weakly magnetized plasma with finite shielding length*, Plasma Phys. Control. Fusion **49** 1719-1733 (2007).

[6] I.H. Hutchinson and L. Patacchini, *Flowing plasmas and absorbing objects: analytic and numerical solutions culminating 80 years of ion collection theory*, Plasma Phys. Control. Fusion **52** 124005 (2010).

[7] I.H. Hutchinson, *Principles of Plasma Diagnostics*, 2nd ed. (Cambridge University press, Cambridge, UK, 2002).

[8] H.K. Mott-Smith and I. Lamngmuir, *The Theory of Collectors in Gaseous Discharges*, Phys. Rev. **28** 727 (1926).

[9] M. Kanal, *Theory of Current Collection of Moving Spherical Probes*, Sci. Report JS-5, Space Physics Research Lab., Univ. of. Mich. (1962).

[10] K.U. Riemann, *The Bohm criterion and sheath formation*, J. Phys. D **24** 493-518 (1991).

[11] J.G. Laframboise, *Theory of spherical and cylindrical Langmuir probes in a collisionless Maxwellian plasma at rest*, Technical report 100, PhD thesis, University of Toronto Institute for Aerospace Studies (1966).

[12] L.J. Sonmor and J.G. Laframboise *Exact current to a spherical electrode in a collisionless, large Debye-length magnetoplasma*, Phys. Fluids **3**, 2472-2490 (1991).

[13] L. Patacchini and I.H. Hutchinson, *Kinetic solution to the Mach probe problem in transversely flowing strongly magnetized plasmas*, Phys. Rev. E **80**, 036403 (2009).

[14] I.H. Hutchinson, *Ion Collection by Oblique Surfaces of an Object in a Transversely Flowing Strongly Magnetized Plasma*, Phys. Rev. Lett. **101** 035004 (2008).

[15] B. Lipschultz, D. Whyte, B. LaBombard, *Comparison of particle transport in the scrape-off layer plasmas of Alcator C-Mod and DIII-D*, Plasma Phys. Control. Fusion **47**, 1559-1578 (2005).

[16] V. Nosenko, R. Fisher, R. Merlino *et al*, *Measurement of the ion drag force in a collisionless plasma with strong ion-grain coupling*, Phys. Plasmas **14**, 103702 (2007).

[17] A.Yu. Pigarov, S.I. Krasheninnikov, T.K.Soboleva *et al*, *Dust-particle transport in tokamak edge plasmas*, Phys. Plasmas, **12** 122508 (2005).

[18] V.E. Fortov, A.C. Ivlev, S.A. Khrapak *et al Complex (dusty) plasmas: Current status, open issues, perspectives*, Physics reports **421** 1-103 (2005).

[19] I.H. Hutchinson, *A fluid theory of ion collection by probes in strong magnetic fields with plasma flow*, Phys. Fluids **30** 3777 (1987).

[20] J.P. Gunn and V. Fuchs, *Mach probe interpretation in the presence of suprathermal electrons*, Phys. Plasmas **14** 032501 (2007).

[21] R.W Hockney and J.W. Eastwood, *Computer simulation using particles*, Taylor and Francis (1989).

[22] C.K. Birdsall and A.B. Langdon, *Plasma Physics via computer simulation*, Institute of Physics, Series in Plasma Physics (1991).

[23] W.H. Press and S.A. Teukolsky and W.T. Vetterling and B.P. Flannery, *Numerical Recipes (3^d edition)*, (Cambridge University Press, NY, 2001).

[24] N. Singh, W.C. Leung and G.M. Singh, *Enhanced current collection by a positively charged spacecraft*, J. Geophysical Research, 105 **A9** 20935-20947 (2000).